Marine and Petroleum Geology 26 (2009) 916–927

Contents lists available at ScienceDirect

Marine and Petroleum Geology

journal homepage: www.elsevier.com/locate/marpetgeo

The importance of shale composition and pore structure upon gas storage potential of shale gas reservoirs

Daniel J.K. Ross*, R. Marc Bustin

Department of Geological Sciences, University of British Columbia, 6339 Stores Road, Vancouver, BC V6T 1Z4, Canada

ARTICLE INFO

Article history:
Received 30 August 2007
Received in revised form 7 June 2008
Accepted 18 June 2008
Available online 25 June 2008

Keywords:
Pore structure
Microporosity
Sorption
Shale gas reservoirs

ABSTRACT

The effect of shale composition and fabric upon pore structure and CH_4 sorption is investigated for potential shale gas reservoirs in the Western Canadian Sedimentary Basin (WCSB). Devonian–Mississippian (D–M) and Jurassic shales have complex, heterogeneous pore volume distributions as identified by low pressure CO_2 and N_2 sorption, and high pressure Hg porosimetry. Thermally mature D–M shales (1.6–2.5% VRo) have Dubinin–Radushkevich (D–R) CO_2 micropore volumes ranging between 0.3 and 1.2 cc/100 g and N_2 BET surface areas of 5–31 m^2/g. Jurassic shales, which are invariably of lower thermal maturity ranging from 0.9 to 1.3% VRo, than D–M shales have smaller D–R CO_2 micropore volumes and N_2 BET surface areas, typically in the range of 0.23–0.63 cc/100 g (CO_2) and 1–9 m^2/g (N_2).

High pressure CH_4 isotherms on dried and moisture equilibrated shales show a general increase of gas sorption with total organic carbon (TOC) content. Methane sorption in D–M shales increases with increasing TOC and micropore volume, indicating that microporosity associated with the organic fraction is a primary control upon CH_4 sorption. Sorption capacities for Jurassic shales, however, can be in part unrelated to micropore volume. The large sorbed gas capacities of organic-rich Jurassic shales, independent of surface area, imply a portion of CH_4 is stored by solution in matrix bituminite. Solute CH_4 is not an important contributor to gas storage in D–M shales. Structural transformation of D–M organic matter has occurred during thermal diagenesis creating and/or opening up microporosity onto which gas can sorb. As such, D–M shales sorb more CH_4 per weight percent (wt%) TOC than Jurassic shales.

Inorganic material influences modal pore size, total porosity and sorption characteristics of shales. Clay minerals are capable of sorbing gas to their internal structure, the amount of which is dependent on clay-type. Illite and montmorillonite have CO_2 micropore volumes of 0.78 and 0.79 cc/100 g, N_2 BET surface areas of 25 and 30 m^2/g, and sorb 2.9 and 2.1 cc/g of CH_4, respectively (dry basis) – a reflection of microporosity between irregular surfaces of clay platelets, and possibly related to the size of the clay crystals themselves. Mercury porosimetry analyses show that total porosities are larger in clay-rich shales compared to silica-rich shales due to open porosity associated with the aluminosilicate fraction. Clay-rich sediments (low Si/Al ratios) have unimodal pore size distributions $<$10 nm and average total porosities of 5.6%. Siliceous/quartz-rich shales (high Si/Al) exhibit no micro- or mesopores using Hg analyses and total porosities average 1%, analogous to chert.

1. Introduction

1.1. Shale pore structure

Elucidating the pore structure, sorption characteristics and potential gas capacities of organic-rich shales is important due to potentially significant gas contents of shale gas reservoirs (Montgomery et al., 2005; Bustin, 2005a; Pollastro, 2007; Ross and Bustin, 2007, 2008). In the Western Canadian Sedimentary Basin (WCSB) alone, shale gas resources (which includes gas from mudstones, siltstones, tight sands and marlstones) are estimated to be $>$1000 trillion cubic feet (tcf; Bustin, 2005a,b). To reduce exploration risk and determine economic feasibility, knowledge of gas storage and transport mechanisms is required so producible resources can be quantified and long-term production behaviour be evaluated. However, there is a lack of data in the literature which addresses the relationship between porosity, pore size distribution and total gas capacity in shales. Resource evaluations are complicated by the structurally heterogeneous nature of fine-grained strata and their intricate pore networks, which are interdependent on many geologic factors including total organic carbon (TOC) content, mineralogy, maturity and grain-size (Yang and Aplin, 1998;

* Corresponding author. Present address: Unconventional Gas Team, Shell Canada Limited, 400 4th Avenue S.W., P.O. Box 100 Station M, Calgary, Alberta T2P 2H5, Canada. Tel.: +1 11 403 384 5763; fax: +1 11 403 384 6499.
E-mail address: daniel.ross@shell.com (D.J.K. Ross).

0264-8172/$ – see front matter © 2008 Elsevier Ltd. All rights reserved.
doi:10.1016/j.marpetgeo.2008.06.004

Dewhurst et al., 1999a,b; Ross, 2004; Ross and Bustin, 2007; Chalmers and Bustin, 2007a).

In previous shale gas studies, sorbed[1] CH_4 capacities correlate with TOC (Manger et al., 1991; Lu et al., 1995; Ross and Bustin, 2007), although the reasoning for this relationship is unclear because the pore structure of liptinite macerals (marine organic matter) is poorly constrained. Chalmers and Bustin (2007a) reported an increase of CH_4 sorption capacity with an increase in micropore volume for Cretaceous shales, akin to coalbed methane (CBM) reservoirs (Lamberson and Bustin, 1993; Crosdale et al., 1998; Clarkson and Bustin, 1999). Microporosity,[2] which is positively correlated with TOC in shales (Chalmers and Bustin, 2007a), is a critical component of porous media (e.g. zeolites, activated carbons) due to large internal surface areas and greater sorption energies of sub-2 nm pores compared to larger pores of solids with similar composition (Dubinin, 1975).

In an attempt to elucidate the complex pore structure of shales, researchers have utilized low pressure N_2 sorption isotherms, He pycnometry and Hg porosimetry (Katsube and Williamson, 1994; Yang and Aplin, 1998; Katsube et al., 1998; Eseme et al., 2006). Pore size distributions and total pore volumes of shales and mudrocks are also reported under variable confining pressures and effective stresses (e.g. Mondol et al., 2007), to better understand hydraulic conductivity/permeability and sealing efficiency of cap rocks. Sealing efficiency has been found to be dependent on clay mineral surface area (Yang and Aplin, 1998; Dewhurst et al., 1999a). Aluminosilicate phases can have nanometre scale pore structures (hence large surface area; Aylmore and Quirk, 1967; Lloyd and Conley, 1970; Aylmore, 1974; Fripiat et al., 1974; Gil et al., 1995; Altin et al., 1999; Aringhieri, 2004; Wang et al., 2004) and may provide sorption sites for CH_4 in addition to the organic fraction (e.g. Manger et al., 1991; Lu et al., 1995; Cheng and Huang, 2004).

1.2. Coals as analogues

Shale gas and CBM reservoirs are informally grouped as unconventional or non-conventional because gas is trapped in part by sorption processes in low permeability strata (Law and Curtis, 2002). Geologic controls on CBM reservoir capacities are well documented. Important coal properties include maceral type (Lamberson and Bustin, 1993; Crosdale et al., 1998), ash content (Laxminarayana and Crosdale, 1999), rank (Clarkson and Bustin, 1999; Laxminarayana and Crosdale, 1999, 2002; Hildenbrand et al., 2006), moisture (Joubert et al., 1974; Unsworth et al., 1989; Levy et al., 1997) and temperature (Bustin and Clarkson, 1998; Azmi et al., 2006). Crosdale et al. (1998) argued maceral type and rank are critical factors controlling gas sorption because of their influence on pore structure and consequently the sorption process. Chalmers and Bustin (2007b) showed that high pressure solubilization of CH_4 was responsible for large gas capacities of liptinite-rich coals (bituminite and gilsonite). Mastalerz et al. (2004) found no relationship between liptinite content in coal and gas sorption which we attribute to the low concentrations of marine organic matter in the coals they examined.

Although previous studies have provided useful insight to CH_4 sorption in organic-rich strata, direct comparisons of sorption characteristics between coals and shales may be of limited use due to physio-chemical differences that include

(1) Type of organic matter: coals are typically enriched in vitrinite/inertinite macerals as oppose to liptinite-rich shales.
(2) % Organic matter.
(3) % Mineral matter.
(4) Porosity (total pore volume and pore size distribution).

The objectives of the current study are to investigate the porosity characteristics (pore structure and total porosity) of shale gas reservoirs, which impact both gas sorption processes and the total gas capacities. Our findings will aid reservoir model estimates of total gas resources and provide insight to the release of CH_4 from shale matrices to predict gas transport. In this paper, we examine the effects of various shale attributes (organic/inorganic composition, thermal maturity) upon pore structure and high pressure CH_4 sorption and potential total gas capacity.

2. Methods

2.1. Samples and preparation

A suite of Jurassic and Devonian–Mississippian (D–M) shales from northern British Columbia, western Canada, were chosen for this study due to their variability of (1) TOC contents; (2) inorganic composition and (3) thermal maturity – attributes which ultimately control the gas storage potential of unconventional gas reservoirs. These shales are currently being explored as shale gas reservoirs, hence an understanding of gas storage controls is important for estimating gas capacities and booking reserves (Ross and Bustin, 2007, 2008). Devonian–Mississippian samples are taken from the organic-rich Muskwa and Besa River formations and the organic-lean Fort Simpson Formation. The Besa Formation is subdivided into three informal units (Ross and Bustin, 2008): (1) lower black mudrock (LBM) member; (2) middle shale member (MS) and (3) upper black shale (UBS) member. The LBM and UBS members are examined in this study.

Within northern British Columbia, Devonian–Mississippian shaly strata have undergone a complex, multiphase geothermal history. The Besa River shales are located west of the Bovie Fault, across which strata are displaced by >1200 m over a horizontal distance of 0.5 km (Wright et al., 1994). As a result of burial depth and high Paleozoic geothermal gradients (65 °C/km; Majorowicz et al., 2005), Upper Besa River shales examined in this study have equivalent thermal maturities >2% VRo (Morrow et al., 1993; Stasiuk and Folwer, 2004). As such, Rock Eval pyrolysis data yields no distinct S2 peak despite TOC values of up to 5.7 wt%, highlighting the over-mature nature of Besa River shales (Ross and Bustin, 2008). No vitrinite reflectance data is available for LBM samples, but is estimated to be similar to UBS samples due to comparable burial depth and geothermal gradient. Muskwa samples examined here have VRo between 1.6 and 1.7% (Potter et al., 2000, 2003; Stasiuk and Fowler, 2004). There is limited thermal maturation data available for Fort Simpson shales, due to lack of vitrinite particles and low total organic carbon (TOC) contents (hence poor Rock Eval results; Ross and Bustin, 2008). However, Fort Simpson shales lie conformably upon Muskwa shales in northern BC, and are therefore deemed to have comparable VRo ranges.

Jurassic Gordondale Member shales were included in this study due to high TOC and wide ranges of thermal maturity compared to D–M shales (Ross and Bustin, 2006, 2007). Hence these strata provide additional insight to the relationship between organic matter and shale micropore structure. The affect of mineralogy upon pore size distribution (Hg porosimetry) and total pore volume for Gordondale Member shales is discussed in Ross and Bustin (2007), and therefore not included in this paper.

To investigate the effect of inorganics upon shale pore structure, pure clay mineral standards of illite (IMt-2), kaolinite (KGa-1b) and

[1] Sorption is a general term which includes surface adsorption, absorption and capillary condensation (Gregg and Sing, 1982): adsorption refers to the physical uptake of gas by pore volume filling or monolayer formation; absorption refers to the incorporation or assimilation of gas molecules into the solids lattice.

[2] Following the International Union of Pure and Applied Chemistry (IUPAC) pore classification (Rouquerol et al., 1994), micropores are <2 nm diameter, mesopores are between 2 and 50 nm, and macropores are >50 nm.

chlorite (clinochlore, CCa-2), representative of the clay minerals of shales analyzed in this study and Na-saturated montmorillonite (SWy-2) were obtained from the University of Missouri-Columbia Source Clay Minerals Repository. The loose clay standard aggregates provide useful analogues to the clay component within the shales because pore structure analyses of shales are also conducted upon crushed samples (<250 μm) and the surface areas being investigated are at a scale in which macro-fabric plays little role. Therefore the impact of sedimentary fabric upon gas diffusion and sorption in the shales is reduced (but not completely removed). The pore structure of Devonian chert (northern British Columbia) was also analyzed to assess the impact of biogenic silica on pore structure since silica in Muskwa and LBM samples is biogenically sourced and some rocks grade to chert in terms of silica content (Ross and Bustin, in review).

Samples of 150 g were crushed to <250 μm for high pressure CH_4 sorption analysis. A split of approximately 0.2 g was used for low pressure isotherm analysis (CO_2 and N_2 surface area measurements), and 18 g for high pressure Hg porosimetry. Crushed samples were utilized for qualitative petrographic analysis. Due to the required degassing of samples prior to pore structure analyses (CO_2 and N_2 low pressure sorption, Hg porosimetry), pore structure data is reported on a dry basis. Samples were oven dried for 24 h at 110 °C. High pressure CH_4 isotherms were conducted on dry and moisture equilibrated samples. Moisture equilibration of shale samples followed the American Society for Testing and Materials (ASTM) procedure (ASTM D1412-04, 2004). Moisture capacities were determined at 30 °C (the temperatures at which high pressure CH_4 isotherms were measured) using weight loss calculations by oven-drying, as recommended for moisture content under reservoir conditions by the ASTM. This method consisted of equilibrating crushed shale samples in a sub-atmospheric desiccator over a saturated solution of potassium sulphate for more than 72 h.

It may seem counter-intuitive to compare analyses for dry and moisture equilibrated samples as moisture acts as a dilutent to gas sorption (Yee et al., 1993) and its effects cannot easily be isolated. However, the good correlation between CH_4 sorption capacity under dry and moisture equilibrated states (Fig. 1) suggests meaningful comparisons can be made. The controls on moisture contents and its effect on sorption capacity in shale gas reservoirs will be addressed specifically in a future paper.

2.2. Low pressure CO_2 and N_2 isotherm analyses

Low pressure CO_2 and N_2 isotherms (<0.127 MPa) are used to describe the pore space of organic-rich, microporous materials as

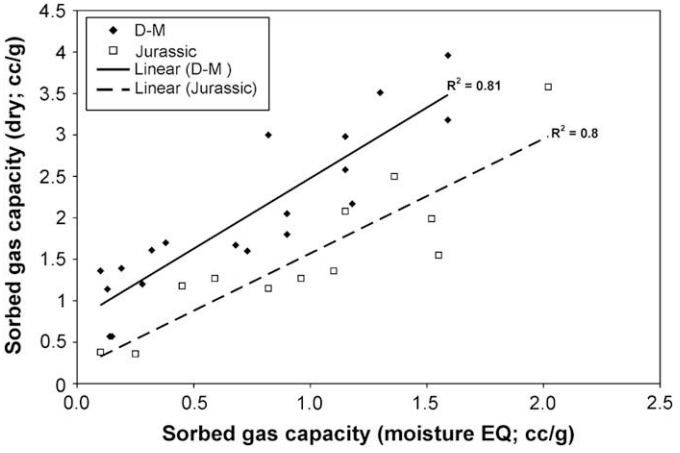

Fig. 1. Correlation between sorption capacities (cc/g) of moisture equilibrated and dry shales examined in this study (D–M = Devonian–Mississippian).

average pore size distributions are in the nanometre scale, into which gases can effectively penetrate (Gan et al., 1972; Dubinin, 1975, 1989; Lamberson and Bustin, 1993; Larsen et al., 1995; Clarkson and Bustin, 1996, 1999; Levy et al., 1997; Bustin and Clarkson, 1998; Prinz and Littke, 2005; Chalmers and Bustin, 2007a,b). Carbon dioxide and N_2 sorption analyses were performed using a Micromeritics® ASAP 2010 surface area analyzer. Carbon dioxide sorption was calculated over a pressure range of 4×10^{-4}–3.2×10^{-2} at 0 °C and monolayer capacities were determined using the Dubinin–Radushkevich (D–R) equation (Gregg and Sing, 1982):

$$\log V = \log V_0 - S \log^2\left(\frac{P}{P_0}\right) \quad (1)$$

where V is the volume of sorbed gas at equilibrium pressure ($cm^3\,g^{-1}$, s.t.p.), V_0 is the total micropore volume ($cm^3\,g^{-1}$, s.t.p.), S is a constant, P is pressure and P_0 is saturation vapour pressure. Micropore volumes were measured by the volume of the adsorbed CO_2 (which completely fills the micropores), expressed in terms of bulk liquid at atmospheric pressure and 0 °C temperature (Rouquerol et al., 1994). As discussed by Dubinin and Stoeckli (1980), the theory of volume filling of micropores is a rational basis for the description of microporous structures in carbonaceous materials. Micropore volumes were calculated using $17 \times 10^{-20}\,m^2$ for the cross-sectional area of the CO_2 molecule and reported as volume per 100 g (cc/100 g). Carbon dioxide sorption data is also reported as equivalent surface area (m^2/g; Tables 1 and 2), so that surface areas can be compared with N_2 and Hg surface areas.

Nitrogen isotherms were measured at −196.15 °C, and equivalent surface areas (m^2/g) calculated using the BET (Brunauer–Emmett–Teller) method in the 0.06–0.2 relative pressure range (P/P_0, where P is the gas vapour pressure in the system and P_0 is the vapour pressure above the gas at the temperature of interest), following the equation (Brunauer et al., 1938):

$$1/W((P_0/P) - 1) = 1/W_m C + C - 1/W_m C(P/P_0) \quad (2)$$

where W is the weight of the sorbed gas at relative pressure P/P_0, W_m is the weight of the monolayer adsorbent (N_2), C is the BET constant which relates to the sorption energy between adsorbent and adsorbate.

The calculated surface area for both low pressure N_2 and CO_2 sorption analyses is a function of the sorption measurements and how the sorption data is interpreted; hence the term *equivalent* surface area is used (herein referred to as surface area; Sing et al., 1985).

2.3. High pressure Hg porosimetry

Mercury intrusion data was collected on a Micromeritics® Autopore IV 9500 Series. Pressure of Hg was increased continuously from 0.013 to 430 MPa and pore size distributions were determined using the Washburn equation (Washburn, 1921):

$$D = \frac{-4\gamma \cos\theta}{P} \quad (3)$$

where D is the pore diameter, γ is the surface tension, θ is the contact angle and P is the applied pressure. A contact angle of 130° (Gan et al., 1972) and surface tension of 485 dyn/cm (Gregg and Sing, 1982) were used. Porosities were calculated from Hg intrusion data.

2.4. High pressure CH_4 isotherm analysis

High pressure CH_4 sorption isotherms at 30 °C were collected using a volumetric Boyles Law apparatus. Sorbed gas capacities

Table 1
Composition, surface areas, thermal maturity and sorption capacities of D–M shales.

Sample ID	TOC* (wt%)	Pore structure/surface area data				Moisture (wt%)	Sorbed gas capacity		Maturity data** (VRo %)	Inorganic composition data**			
		Hg porosity* (%)	N_2 BET surface area (m^2/g)	CO_2 micropore volume (cc/100 g)	CO_2 equivalent surface area (m^2/g)		Moisture EQ (cc/g at 6 MPa)	Dry (cc/g at 6 MPa)		SiO_2 (%)	Al_2O_3 (%	Si/Al (%)	CaO (%)
MU1416-1	2.1	4.4	19.5	0.8	28.9	3.2	0.9	2.1	1.6	64.1	17.5	3.7	0.8
MU1416-4	1.7	2.2	10.1	0.6	23.7	3.5	0.7	–	1.6	65.8	14.7	4.5	0.7
MU1416-7	2.1	2.2	9.1	0.8	29.2	3.5	1.2	2.2	1.6	68.6	12.7	5.4	0.6
MU1416-9	0.4	1.4	3.4	0.3	11.1	2.5	0.2	0.6	1.6	5.5	1.7	3.3	44.6
MU714-3	1.6	1.0	10.5	0.5	18.8	1.9	0.7	1.7	1.7	36.6	7.2	5.1	16.4
MU414-1	3.7	3.7	10.7	1.0	36.7	3.1	0.8	–	n/a	73.5	9.9	7.4	0.6
UBS-C15-1331-1	1.4	5.4	16.8	0.5	19.1	2.4	0.3	1.6	2.5	78.3	9.9	7.9	1.2
UBS-C15-1331-5	4.0	6.0	44.5	1.3	47.2	4.1	1.6	3.2	2.5	60.7	16.9	3.6	0.6
UBS1331-4	4.0	7.2	29.3	0.9	32.9	4.9	1.2	3.0	2.5	47.3	23.0	2.1	1.2
UBS1331-5	4.9	5.1	20.0	1.0	38.3	4.4	1.3	3.5	2.5	50.9	24.1	2.1	0.6
UBS1331-6	4.7	5.2	31.0	1.2	44.7	4.1	1.6	4.0	2.5	45.1	22.3	2.0	1.2
UBS1331-11	3.8	4.6	22.3	0.8	29.8	5.2	0.8	3.0	2.5	48.0	22.9	2.1	0.8
LBM325-1	2.0	1.2	10.3	0.5	17.6	1.6	0.6	–	n/a	82.4	5.7	14.5	0.8
LBM325-5	2.1	1.3	12.8	0.5	18.2	1.8	0.7	1.6	n/a	78.9	9.6	8.2	0.3
LBM325-7	0.9	0.4	5.5	0.3	9.5	1.5	0.3	–	n/a	30.0	3.0	10.0	19.4
LBM2563-1	4.8	1.6	16.3	1.0	37.6	1.4	1.6	–	n/a	80.7	5.9	13.7	1.2
LBM2563-3	4.4	2.1	12.4	0.8	29.7	1.8	1.2	2.6	n/a	80.2	6.3	12.8	1.2
LBM2563-5	2.8	0.8	13.9	0.6	21.9	2.3	0.8	–	n/a	82.4	6.6	12.5	0.5
LBM2563-7	2.5	1.1	12.3	0.7	25.6	1.9	0.9	1.8	n/a	79.4	7.9	10.1	0.8
FSS 1416-1	0.3	2.6	13.6	0.5	18.0	4.8	0.2	1.4	1.6	56.6	19.5	2.9	1.7
FSS 1416-5	0.2	3.0	15.0	0.5	18.6	3.3	0.1	1.4	1.6	55.5	19.2	2.9	1.8
FSS 5245-1	0.3	4.3	20.5	0.6	22.3	3.1	0.1	0.6	n/a	61.0	19.2	3.2	0.4
FSS 12140-6	0.3	3.9	24.7	0.8	29.5	2.8	0.4	1.7	n/a	59.1	19.8	3.0	0.5
FSS 1238-1	0.3	2.5	10.4	0.4	15.9	2.5	0.1	1.1	n/a	56.6	20.6	2.7	1.0
FSS 947-3	0.2	1.9	11.3	0.4	14.9	2.4	0.3	1.2	n/a	40.4	12.9	3.1	17.0

Total organic carbon (TOC) contents, equilibrium moisture contents (moisture), pore characteristics (total porosity, CO_2 micropore volume and N_2 BET surface area) and sorbed gas capacities (moisture equilibrated and dry-state) are provided. Also shown are the three major oxide groups: SiO_2, Al_2O_3 and CaO, representing quartz, clay and carbonate mineral phases, respectively (*data from Ross and Bustin, in review). Dashes show unavailable data. Silica/Al ratios are provided to differentiate silica associated with quartz and clays. **Maturity data for shale samples taken from Potter et al. (2000, 2003) and Stasiuk and Fowler (2002). Note, samples with no available VRo data are shown as n/a.

were calculated from the Peng–Robinson equation of state. The isotherm equation used to model CH_4 sorption is the Langmuir isotherm (Langmuir, 1918):

$$\frac{P}{V} = \frac{1}{BV_m} + \frac{P}{V_m} \tag{4}$$

where P is the equilibrium gas pressure, V is the volume of gas sorbed, V_m is the Langmuir monolayer volume and B is an empirical constant. According to the Langmuir sorption theory, a plot of P vs. P/V produces a straight line and the reciprocal of the slope of the fitted-line relates to the CH_4 monolayer volume. Methane sorption capacities of D–M and Jurassic shales are measured at a consistent temperature (T; 30 °C) and up to a consistent pressure (P; 6 MPa). Although such conditions are not necessarily indicative of subsurface reservoir conditions, these parameters are kept constant so that a meaningful comparison can be made between D–M and Jurassic samples with CO_2, N_2 and Hg pore structure analyses (which are also measured at constant TP conditions).

2.5. Geochemical analyses

Powdered D–M shale and Jurassic samples (15–25 mg) were analyzed for total carbon (TC) using a Carlo Erba® NA-1500 Analyzer (precision of ±2%). Inorganic carbon concentration (IC) values

Table 2
Composition, surface areas and sorption capacities of Jurassic shales.

Sample ID	TOC[a] (wt%)	Pore structure/surface area data				Moisture[a] (wt%)	Sorbed gas capacity		Maturity data		Inorganic composition data[a]			
		Porosity[a] (%)	N_2 BET surface area (m^2/g)	CO_2 micropore volume (cc/100 g)	CO_2 equivalent surface area (m^2/g)		Moisture EQ (cc/g at 6 MPa)	Dry (cc/g at 6 MPa)	T_{max}[a] (°C)	VRo (%) (equivalent)	SiO_2 (%)	Al_2O_3 (%)	Si/Al (%)	CaO (%)
N5378-11	1.6	–	9.3	0.6	21.9	–	–	–	–	–	–	–	–	–
N8354-11	26.6	–	0.0	0.5	19.4	–	–	–	–	–	–	–	–	–
N8354-4	37.8	–	1.6	0.6	23.7	–	–	–	446	0.9	24.8	5.4	4.6	26.8
N376-1	1.4	0.5	0.6	0.2	6.2	0.7	0.1	0.4	494	1.8	18.8	3.2	5.9	24.5
N2557-2	3.1	2.6	1.8	0.2	8.4	2.3	0.1	–	442	0.7	65.0	0.4	16.2	6.7
N6080-1	4.3	2.8	2.8	0.5	18.5	8.5	0.3	0.4	462	1.3	54.9	15.2	3.6	1.2
N3773-2	5.0	0.5	6.3	0.8	28.8	1.8	1.2	2.1	608	2.5	63.9	5.8	11.1	8.6
N89-1	5.2	0.8	2.8	0.3	12.7	1.6	0.5	1.2	457	1.1	16.8	5.5	3.1	35.0
N230-1	7.1	2.2	1.5	0.3	11.4	2.5	0.6	1.3	447	0.9	42.7	11.3	3.8	14.3
N3793-1	9.0	–	1.7	1.1	40.3	2.8	2.0	3.6	607	2.5	47.3	8.5	5.5	13.8
N49-2	10.0	1.5	2.8	0.6	23.4	2.3	1.5	2.0	461	1.2	38.0	7.6	5.0	18.2
N91-1	10.2	4.2	2.3	0.4	15.3	0.6	1.0	1.3	467	1.3	62.9	1.0	62.9	11.5
N174-1	11.8	–	1.2	0.4	16.1	1.7	1.6	1.6	459	1.1	61.0	1.3	45.8	11.7

Included are T_{max} values (and vitrinite reflectance equivalent, % Ro) representing thermal maturation levels.
[a] Data from Ross and Bustin (2007).

were generated from a CM5014 CO_2 coulometer with a precision of 2%. Total organic carbon values were determined by subtracting total inorganic carbon from total carbon values (TOC = TC – IC). Major elements SiO_2, Al_2O_3 and CaO were determined by X-ray fluorescence spectrometry, the precision of results is ±3% (from Ross and Bustin, in review). These major oxides are representative of the main mineral phases: quartz, clays and carbonate. Silica/Al ratios are also included to highlight quartz-rich (high Si/Al ratios) and clay-rich (low Si/Al ratios) samples.

3. Results

Below we firstly clarify the pore structure of D–M and Jurassic shales and then consider the broader implications of the pore structure upon CH_4 sorption and storage. Carbon dioxide, N_2 and Hg analyses are each described separately since the accessibility of pores in microporous materials is dependent upon the molecular size of the fluid – hence different fluids measure different surface areas (as discussed in Section 4; also refer to Rouquerol et al., 1994).

Ultimately, understanding the controls of high pressure CH_4 storage is needed because such analyses determine (1) the degree of gas saturation of both shale gas and CBM reservoirs and (2) the critical desorption pressure (CDP) – the pressure to which the reservoir must be reduced to so that gas can be flowed to the well bore.

3.1. Shale composition

Total organic carbon contents of D–M shales (Besa River, Muskwa and Fort Simpson formations) range between 0.9 and 4.9 wt% (Table 1). Jurassic Gordondale shales have a wider range of TOC than D–M shales, between 3 and 38 wt% (Table 2). The organic fraction is dominated by maceral assemblages of granular micrinite (D–M samples) and matrix bituminite (Jurassic samples; Stach et al., 1982; Teichmüller, 1986). Micrinite, of which bituminite is the progenitor (Stach et al., 1982), is interpreted as the residual organic matter after oil generation and expulsion (Teichmüller and Ottenjann, 1977).

Muskwa and LBM member samples have either high Si/Al ratios or enriched with carbonate (CaO; Table 1). High Si/Al ratios are attributable to quartz content which accounts for 58–93% of the bulk mineralogy (Ross and Bustin, 2008). Carbonate minerals are calcite and dolomite. Upper black shales of the Besa River Formation and Fort Simpson shales are aluminosilicate-rich (low Si/Al) compared to Muskwa, LBM and some Gordondale samples (high Si/Al). The aluminosilicate fraction of the UBS member is dominated by illite and kaolinite, whereas Fort Simpson shales have equal concentrations of illite, kaolinite and chlorite (Ross and Bustin, 2008). The majority of Jurassic shales are aluminosilicate-lean, silica- and/or carbonate-rich (Table 2) with quartz and calcite occurring as the main mineral phases (Ross and Bustin, 2007).

3.2. Low pressure CO_2 analyses – shales

Low pressure D–R CO_2 isotherms of Muskwa and Besa River shales yield micropore volumes which positively correlate with TOC (Fig. 2a). Organic-lean Fort Simpson shales have micropore volumes between 0.4 and 0.79 cc/100 g but sorbed CO_2 capacities show no trend with TOC (Fig. 2a), implying factors other than the organic fraction influence micropore structure. Jurassic shale micropore volumes range from 0.2 to 1 cc/100 g and show no consistent variation with organic content ($r^2 = 0.06$; Table 2, Fig. 2b).

3.3. Low pressure N_2 analyses – shales

Low pressure N_2 isotherms for Jurassic and D–M shales are Type II (Fig. 3), following the classification of Brunauer et al. (1940). Type II isotherms are interpreted of being due to micropore filling at low pressures and multilayer sorption at higher pressures, which suggests some pores are mesoporous (Gil et al., 1995). Unlike the Langmuir Type I isotherm, BET Type II isotherms pass through a monolayer coverage at the second inflection point on the isotherm. The BET isotherm treats different levels of adsorption sites as having differing affinities to sorbing molecules (N_2), where the solid surface influences the monolayer adsorption and subsequent layers being analogous to condensation.

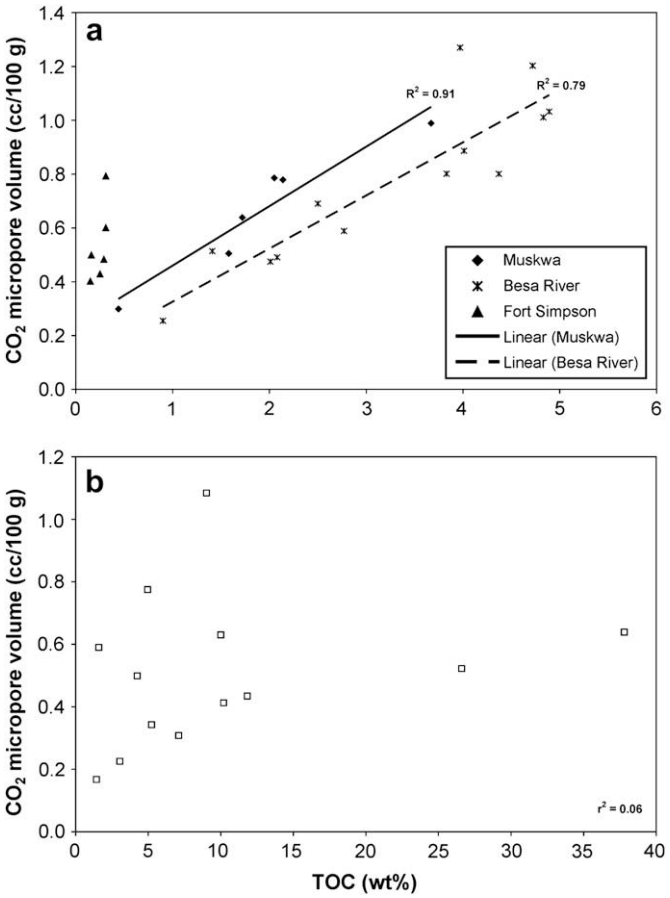

Fig. 2. (a) Relationship between micropore volume and TOC for D–M shales. Note good correlation for Muskwa and Besa River samples and poor correlation for organic-lean Fort Simpson shales ($r^2 = 0.4$, not shown). (b) Variation in micropore volume with TOC for Jurassic shales.

Nitrogen BET surface areas of Besa River and Fort Simpson shales increase with increasing CO_2 micropore volumes, ranging between 5.5 and 44.5 m^2/g (Table 1; Fig. 4). The relationship between BET surface area and micropore volume for Muskwa shales is inconclusive ($r^2 = 0.27$). Nitrogen BET surface areas of Jurassic shales are invariably smaller than D–M shales, varying from 0.04 to 9.3 m^2/g (Table 2), and do not correlate with micropore volume ($r^2 = 0.07$).

3.4. Low pressure CO_2 and N_2 analyses – inorganics

Micropore volume and surface area analyses for clay standards and chert are provided in Table 3. Carbon dioxide micropore volumes are larger for illite (0.79 cc/100 g) and montmorillonite (0.78 cc/100 g) than kaolinite (0.27 cc/100 g) and chlorite (0.13 cc/100 g). Nitrogen BET surface areas range from 4.8 m^2/g (chlorite) to 29.4 m^2/g (illite), correlating with micropore volume (see Section 4.3 for discussions upon clay pore structure). Chert has a small CO_2

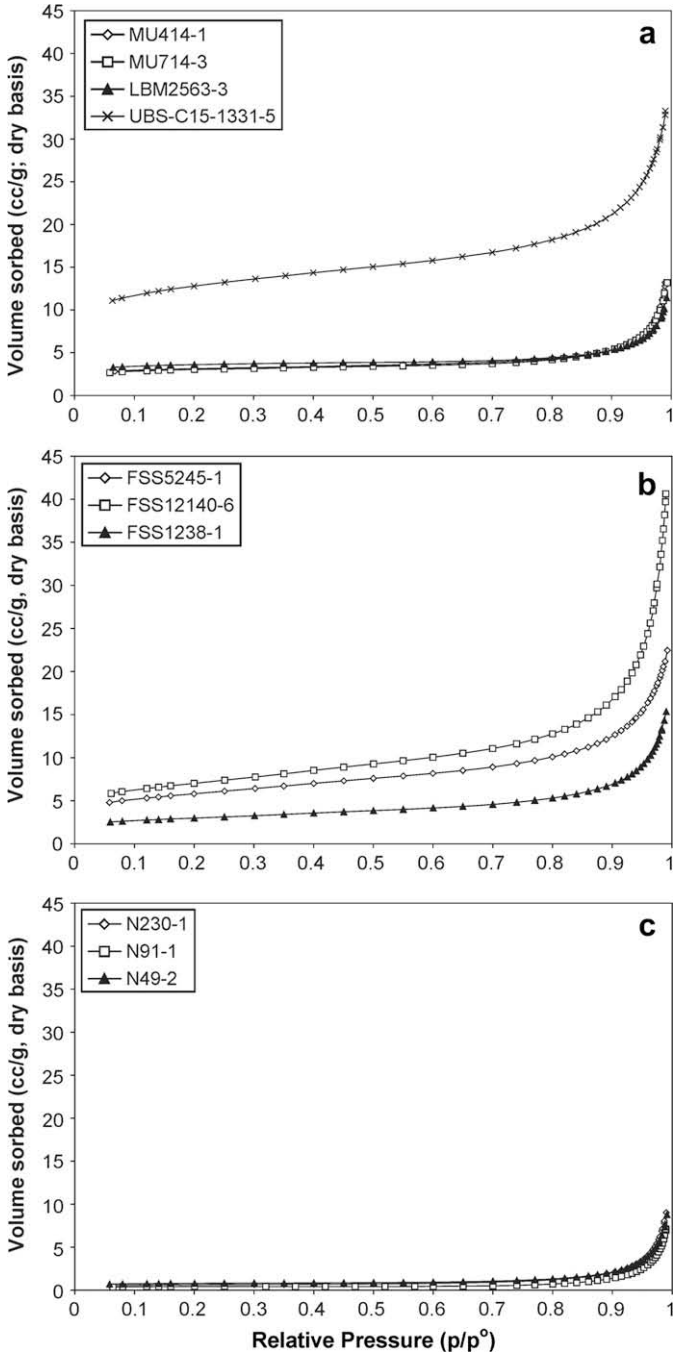

Fig. 3. Low pressure, low temperature (−196.15 °C) N_2 isotherms. (a) Organic-rich Muskwa and Besa River shales; (b) organic-lean Fort Simpson shales; and (c) organic-rich Jurassic shales.

micropore volume (0.08 cc/100 g) and N_2 BET surface area (0.35 m^2/g).

3.5. Porosity and Hg porosimetry

Cumulative pore volumes, in the diameter range of 3–360,000 nm, increase with increasing aluminosilicate content (lower Si/Al ratios). Clay-rich UBS samples have average porosities of 5.6% whereas high Si/Al (high quartz), low clay content LBM samples have average porosities of 1% (Table 1). Average pore size distributions skew towards smaller pores with lower Si/Al ratios (aluminosilicate-rich; Fig. 5). Clay-rich shales have unimodal pore

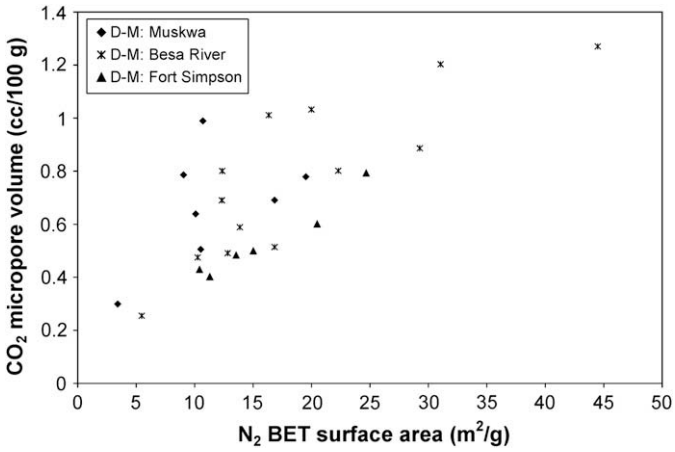

Fig. 4. Correlation between CO_2 micropore volume and N_2 BET surface area for D–M shales (Fort Simpson $r^2 = 0.95$; Besa River $r^2 = 0.69$; Muskwa $r^2 = 0.27$).

diameters of 7–8 nm, in contrast to high Si/Al shales and chert (Fig. 6) which show a dominance of pores >10,000 nm.

Assuming surface areas calculated by Hg injection are primarily a function of meso-macropores (>3 nm diameter; Webb and Orr, 1997), mesopores for N_2 analyses (>2 nm; Unsworth et al., 1989; Rouquerol et al., 1994) and micropores for CO_2 analyses (<2 nm; Marsh, 1989), the contribution from various pore sizes to cumulative specific surface area can be approximated. There is a small amount of surface area associated with pores >15 nm in D–M shales (Fig. 7a). Between 24 and 26% of the total surface area occurs within pores >3 nm for clay-rich, high-porosity UBS samples compared to 2–12% for quartz-rich, low-porosity LBM samples. Carbon dioxide surface areas are >N_2 surface area for D–M shales. Jurassic shales have comparable Hg and N_2 surface areas, and pores >3 nm account for up to 58% of the total surface area (Fig. 7b). Carbon dioxide surface areas are significantly >N_2 surface areas, which may reflect the high solubility coefficient of CO_2 in the matrix bituminite of Jurassic shales (Reucroft and Patel, 1983).

Nitrogen BET surface areas of D–M shales correlate with total porosity (Fig. 8) whereas the correlation between CO_2 micropore volume and total pore volume is poor ($r^2 = 0.2$). No relationship between total porosity, BET surface area and micropore volume could be determined for Jurassic shales.

3.6. High pressure CH_4 analyses

High pressure CH_4 sorption capacities of Jurassic and D–M shales correlate with TOC (moisture equilibrated and dry samples), although the correlation is significantly weaker for Jurassic shales (Fig. 9). Both data sets are approximately linear, going through the origin of the TOC-sorption plot, implying that the TOC is a critical control upon CH_4 sorption and storage. Sorbed gas capacities under moisture equilibration conditions range from 0.1 cc/g for organic-lean shales to 2 cc/g for organic-rich shales. In the dry-state, sorbed gas capacities range from 0.4 to 4 cc/g.

Devonian–Mississippian shales show a positive correlation between TOC, micropore volume and sorbed CH_4 capacity (Fig. 10a), highlighting the microporous nature of the organic matter. A relationship between TOC, micropore volume and sorbed CH_4 capacity for Jurassic shales is not evident (Fig. 10b), suggesting the organic matter in Jurassic shales is not as structured as it is in D–M shales.

Sorbed CH_4 capacities of dry and moisture equilibrated and illite, montmorillonite and kaolinite vary significantly. On a dry basis, illite and montmorillonite have larger sorption capacities than

Table 3
Results of pore structure (CO_2 micropore volume and N_2 BET surface area), moisture and sorbed gas capacities of clay mineral standards and chert.

	Pore structure/surface area data			Moisture (wt%)	Sorbed gas capacity	
	N_2 BET surface area (m^2/g)	CO_2 micropore volume (cc/100 g)	CO_2 equivalent surface area (m^2/g)		Moisture EQ (cc/g at 6 MPa)	Dry (cc/g at 6 MPa)
Clay minerals						
Illite	30.0	0.8	29.4	5.9	0.4	2.9
Montmorillonite	24.7	0.8	28.3	19.0	0.3	2.1
Kaolinite	7.1	0.3	9.8	2.9	0.7	0.7
Chlorite	2.1	0.1	4.8	0.8	–	–
Chert	0.4	0.1	3.12	0	–	–

kaolinite (Fig. 11); a result of greater micropore volume and surface area (Table 3). However, kaolinite sorbs more CH_4 on a moisture equilibrated basis, a consequence of low moisture content (2.9 wt%) compared to illite (5.9%) and montmorillonite (19%).

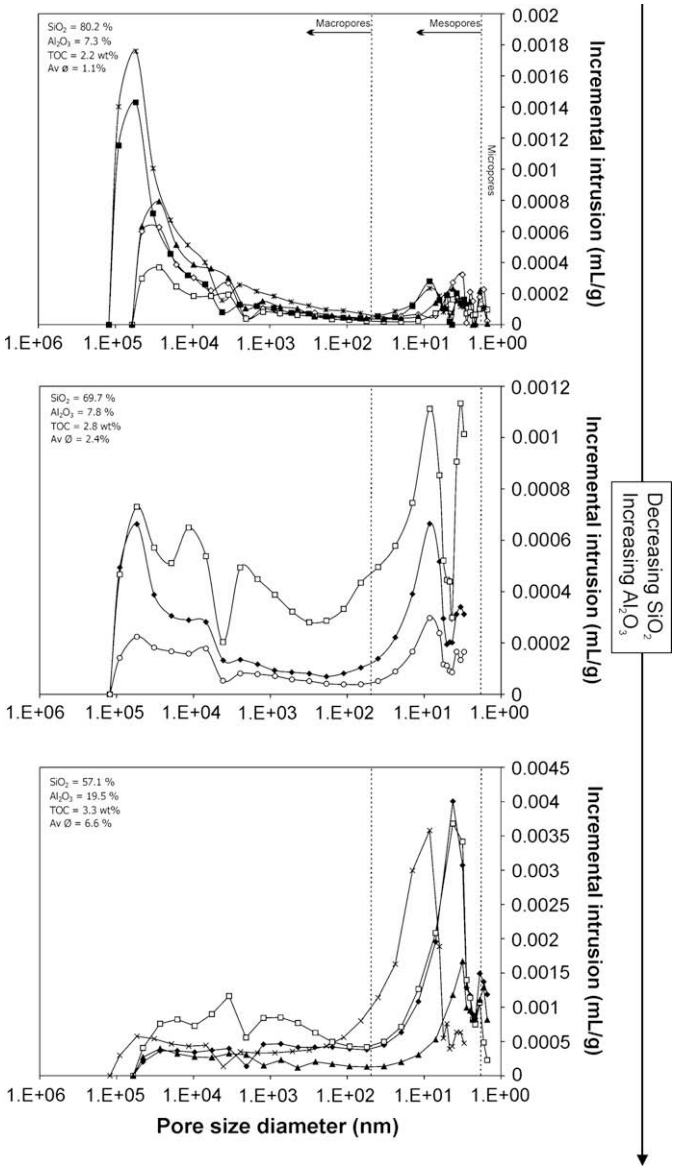

Fig. 5. Relationship between shale composition (quartz and clays), total porosity (Ø) and pore size distribution for D–M shales. Major element geochemistry and total porosity are an average for the samples shown. High silica content shales (top; high Si/Al ratios) are tight with low total pore volume. As aluminosilicate fraction increases (lower Si/Al ratios), porosity increases and modal pore size distribution shifts towards mesopores (microporosity associated with the organic fraction cannot be penetrated by Hg).

4. Discussion – developing a pore structure model

Due to dissimilarities and heterogeneities of their pore structures, Jurassic and D–M strata are discussed separately. In the following sections, the effect of (1) organic matter abundance, type and thermal maturity and (2) mineral matter, upon pore structure and total pore volume are discussed.

4.1. Sorption characteristics and organics: Jurassic strata

Jurassic shales are organically richer than D–M shales but do not show an increase of CO_2 microporosity or N_2 BET surface area with TOC. The ratio of micropore surface area to TOC is lower for Jurassic shales, averaging 4.2 compared to 8.6 for D–M shales. Thus despite the relative importance of organic carbon to sorption capacity (Fig. 9), the influence of TOC upon micropore structure is not as apparent in Jurassic shales, perhaps reflecting the amorphous character of matrix bituminite which comprises a large percentage of the TOC. Significant quantities of CH_4 are stored within organic-rich Jurassic shales, in spite of small micropore volumes, because CH_4 may be solubilised within the matrix bituminite (analogous to solute methane within semi-solid bitumen; Svrcek and Mehrotra, 1982). For example, sample N174-1 sorbs over 300% more CH_4 than N89-1, but N174-1 has only 20% more micropore volume (Table 2; Fig. 10b). The difference in gas capacity is attributable to TOC, which is volumetrically more significant in N174-1 (11.8 wt%) than N89-1 (5.2 wt%), and provides an additional gas storage mechanism (as a solute in the bituminite) to the gas physically adsorbed onto micropore surfaces.

A solute gas component in Jurassic samples is indicated by the linear correlation between pressure and sorption capacity (Fig. 12). Typically, high pressure sorption experiments of microporous materials result in Type I isotherms (as described by Brunauer et al., 1940) due to gas saturation at higher pressures from the completion of a monolayer. Type I isotherms are not indicative of some

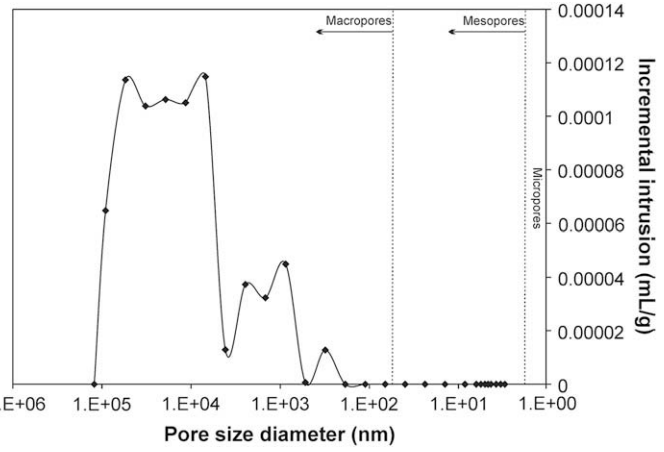

Fig. 6. Mercury incremental intrusion vs. pore diameter for chert. Note comparable pore size distribution to silica-rich LBM samples.

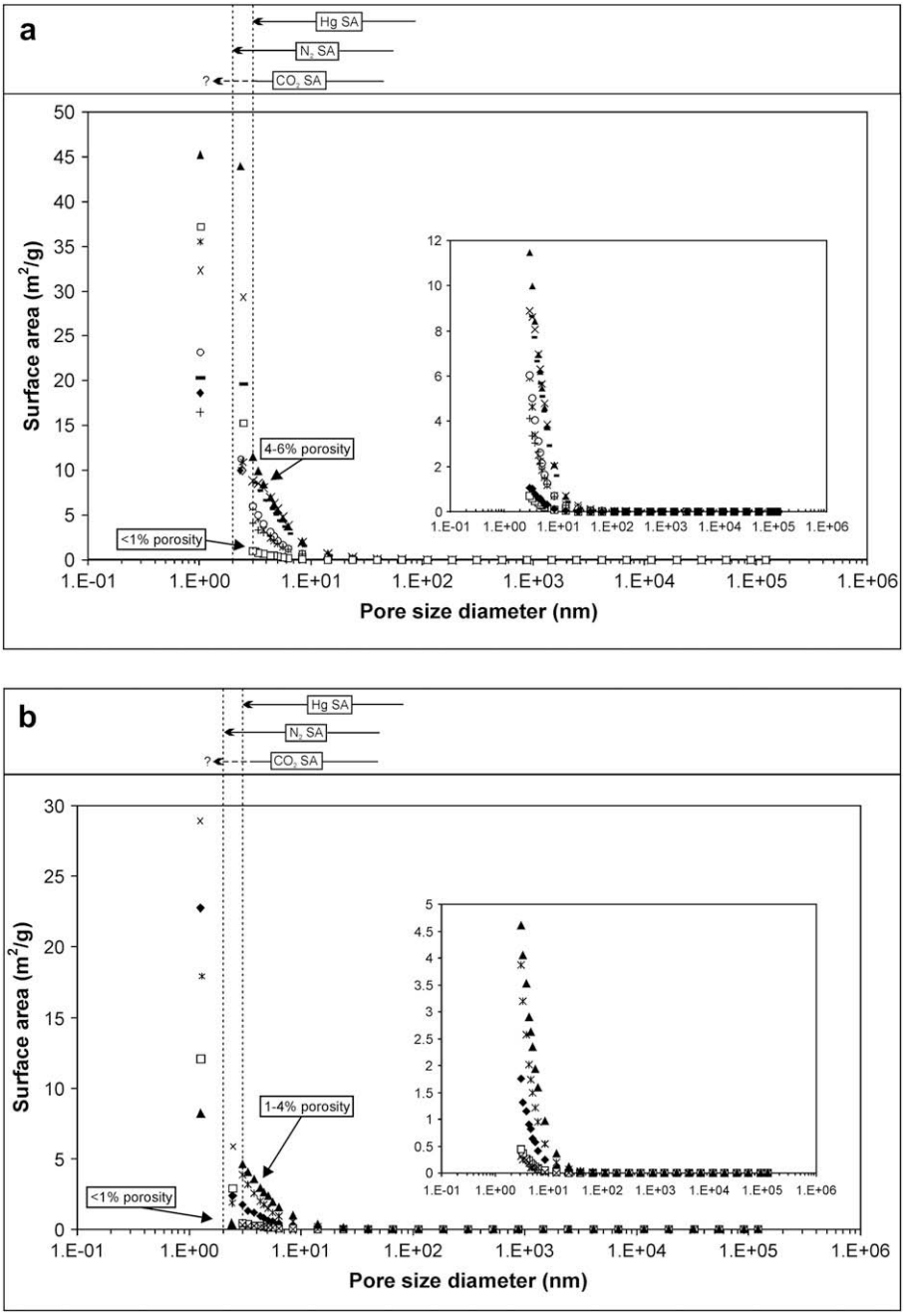

Fig. 7. Comparison of cumulative surface areas calculated using various techniques (low pressure CO_2 and N_2 sorption, high pressure Hg porosimetry). (a) D–M shales: most surface area is associated with pores <10 nm in diameter (SA = surface area). A significant proportion is in pores with pore throat diameters less than 2 nm. (b) Jurassic shales: similar to D–M shales, most surface area is associated with pores <10 nm in diameter. Insets show surface area associated with pores >3 nm diameter.

Jurassic samples as the gas storage process follows Henry's Law (Duffy et al., 1961), where the concentration of solute gas is directly proportional to the partial pressure of that gas above the solution. The inability of CO_2 and N_2 to go into solution (reflected by moderate CO_2 micropore volumes and low N_2 BET surface areas of some high TOC samples) is an artefact of the low pressure analyses in contrast to the high pressure CH_4 analyses.

4.2. Sorption characteristics and organics: Devonian–Mississippian strata

Sorption capacities and micropore volumes of D–M shales increase with TOC, highlighting the greater sorption energy of smaller pores within the organic fraction (Burggraaf, 1999). Nitrogen BET surface areas are covariant with CO_2 micropore volume suggesting high-sorbing samples are both micro- and mesoporous. Gan et al. (1972) argued N_2 cannot access the finest micropores at low temperatures, and hence only measuring the external surface area and area contained within mesopores (Rouquerol et al., 1994). At −196 °C, N_2 lacks the required thermal energy to diffuse through the narrow constricted pore throats (Unsworth et al., 1989). Carbon dioxide, which is used at a higher temperature and thus has greater thermal energy, can force through narrow passages (Larsen et al., 1995) and is believed to represent the 'truest' surface area, measuring microporosity and ultra-microporosity (e.g. <0.5 nm diameter; Marsh, 1989).

The large micropore volumes and surface areas per wt% TOC of D–M shales compared to Jurassic shales are a product of thermal

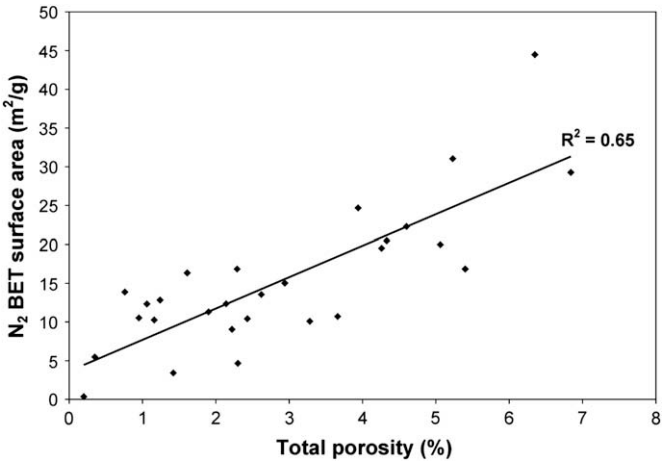

Fig. 8. Moderate correlation between N_2 BET surface area and porosity (measured by Hg porosimetry) suggesting total porosity is influenced by the mesopore structure of D–M shales.

maturation. Jurassic strata in northern British Columbia have equivalent vitrinite reflectances (% Ro) typically <1.2% Ro (Table 2) whilst D–M shales are more thermally mature, with vitrinite reflectance values (actual or equivalent) ranging between 1.6 and 2.5% Ro (Table 1; Morrow et al., 1993; Potter et al., 2000, 2003; Stasiuk and Fowler, 2002). At higher thermal maturity, diagenesis structurally transforms the organic fraction (described here as micrinite), creating more microporosity and/or decreasing the heterogeneity of the pore surfaces: processes related to larger sorbed gas capacities of high-rank coals (e.g. Levy et al., 1997; Bustin and Clarkson, 1998; Laxminarayana and Crosdale, 1999). During coalification, it is believed that the hydrocarbon components are cracked, opening up additional sorption sites to CH_4, hence coal pore volume distribution was argued to be dependent upon the rank of the coal (Gan et al., 1972). Due to these processes, D–M shales sorb more gas per wt% TOC than Jurassic shales. Larger micropore volumes within the Jurassic suite of samples are associated with thermally mature shales (~2.5% VRo; N3773-2 and N3793-1), contributing an adsorbed gas component to the total sorption capacity. These results emphasize the 'over-printing' effect of thermal maturity upon organic matter, pore structure and gas sorption. No consistent variation exists between thermal

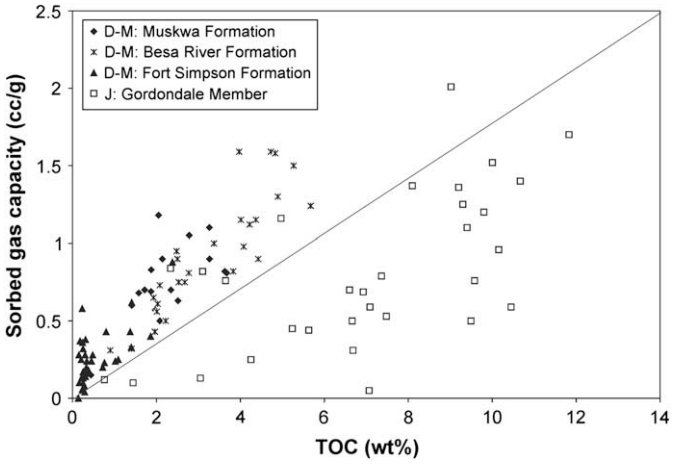

Fig. 9. Correlation between TOC and methane sorption capacity of moisture equilibrated D–M and Jurassic shales. Diagonal line highlights the ratio difference of methane sorption to TOC (Jurassic shales: $r^2 = 0.38$; Fort Simpson shales: $r^2 = 0.46$; Muskwa and Besa River shales: $r^2 = 0.8$).

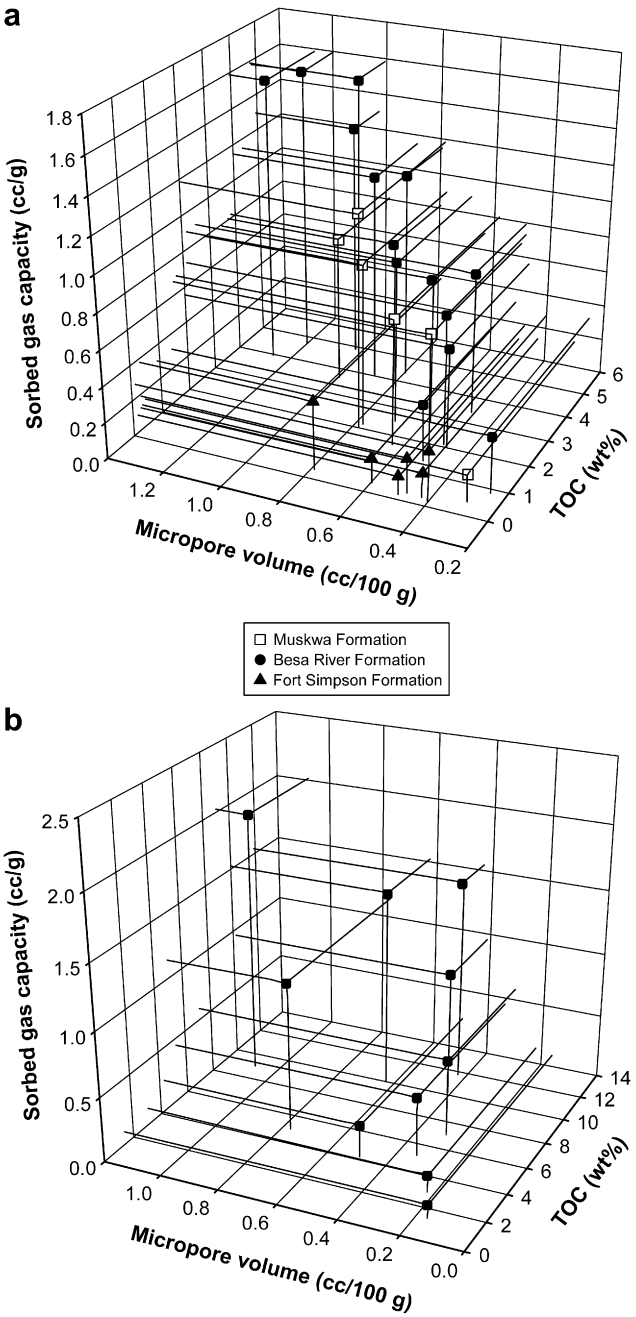

Fig. 10. Three-dimensional plots relating TOC and micropore volume with sorption capacity. (a) D–M shales and (b) Jurassic shales. Note importance of microporous organic material upon gas sorption capacities in D–M shales.

maturation and microporosity as pore structure is affected by other compositional attributes (e.g. inorganic material).

4.3. Sorption characteristics: effect of inorganics upon micropore structure

The influence of mineralogy upon shale pore structure and surface area is evident in D–M shales. Organic-lean, aluminosilicate-rich Fort Simpson shales have micropore volumes which cannot be related to the organic fraction (Fig. 2a). The micropore structure is controlled by the clay fraction (Fig. 13): illite, chlorite and kaolinite (Ross and Bustin, in review), whereas micropore volumes of silica-rich, aluminosilicate-poor LBM samples (>75% SiO_2) are a function of TOC only (Fig. 13). The biogenic silica (Ross

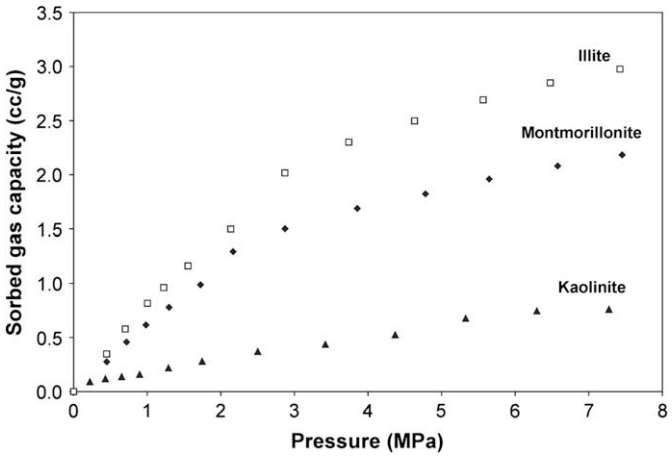

Fig. 11. Sorption isotherms (at 30 °C) for clay standards (dry basis).

and Bustin, in review) has insignificant microporosity and hence sorption sites, as indicated by the small micropore volume and surface area, and no pore sizes <100 nm diameter in chert. Clay-rich UBS samples, which have comparable organic contents and maturity to LBM samples, have the largest micropore volumes and BET surface areas, reflecting a contribution of organics and clays to the micropore structure (Fig. 13). The microporosity of clay minerals can be associated with the degree and type of packing (irregular surfaces between clay plates) and the size of the clay crystals themselves (Aylmore and Quirk, 1967). Importantly, the nature of the exchangeable cations in clays has very little if any significant effect upon gas sorption (Aylmore and Quirk, 1967; Aylmore, 1974), hence the clay mineral standards provide a useful insight to the possible pore structure contribution of clay mineral phases to the shales examined here.

Consideration must also be given to the hydrophilic nature of clay minerals which reduces their adsorptive capacity (Table 3). Under moisture equilibrated conditions, moisture may render many microporous sorption sites unavailable to CH_4 by filling pore throats or occupying sorption sites (Joubert et al., 1973, 1974; Yalçin and Durucan, 1991; Bustin and Clarkson, 1998; Krooss et al., 2002; Hildenbrand et al., 2006; Ross and Bustin, 2007).

In a study of gas sorption on clays, coals and shales, Cheng and Huang (2004) reported comparable CH_4 capacities of pure kaolinite and montmorillonite standards to oil shale (TOC = 20.2 wt%). However, surface areas measured using the N_2 BET method were

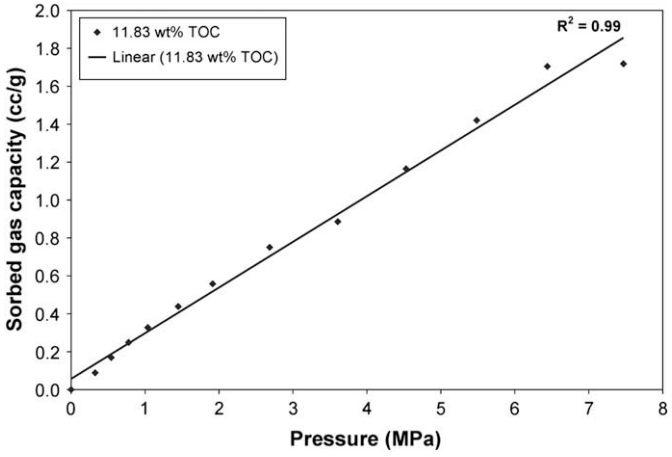

Fig. 12. Linear correlation between pressure and methane sorption of a Jurassic shale sample, indicative of a solute gas (following Henry's Law).

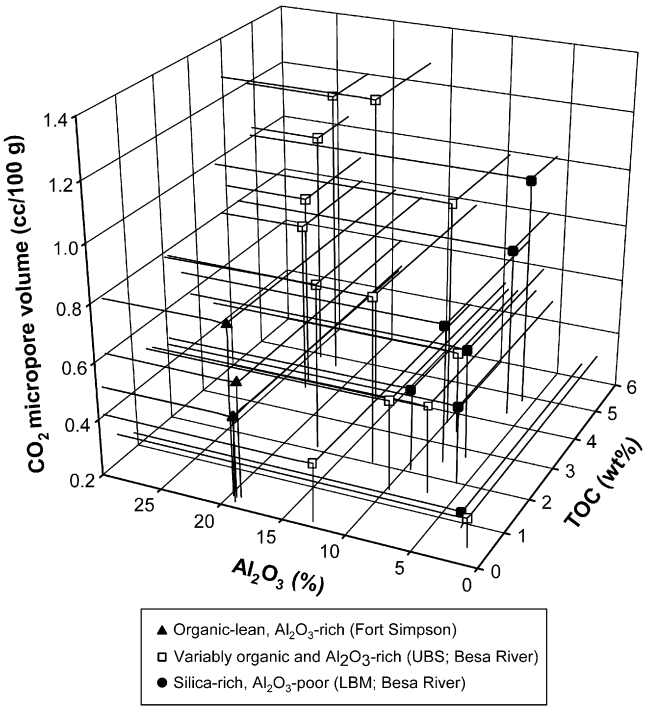

Fig. 13. Variation of micropore volume with TOC and clay fraction (proxied by percent Al_2O_3) for D–M shales. Clay-rich Fort Simpson shales have micropore volumes which are not related to organic contents. Biosiliceous LBM samples show a strong correlation between TOC and micropore volume. Shales enriched in both clays and organics (UBS samples) have the largest micropore volumes, suggesting a micropore contribution from both the organic and clay fractions.

smaller for the oil shale than clay minerals. In an attempt to relate the variation in sorption capacity with surface area, Cheng and Huang (2004) estimated the area coverage of CH_4 concluding absorption in the organics may provide an additional retention mechanism. Devonian–Mississippian shales have microporosities, surface areas and sorbed gas capacities comparable with clay mineral standards, suggesting the influence of absorption is minimal.

4.4. Pore size distribution and total porosity measured by Hg porosimetry

Mercury porosimetry data indicates that inorganic material influences total pore volumes and pore size distributions. High Si/Al (quartz-rich) D–M shales have pore sizes skewed towards smaller pores and lower total pore volumes, most notably for LBM samples. The largest porosities were measured for clay-rich shales (UBS member). These findings are in contrast to other studies which describe porosity increasing with quartz content due to the presence of intergranular pores between coarser detrital grains (silt-sized quartz; Schlömer and Krooss, 1997; Dewhurst et al., 1999b). However, silica in LBM and MU strata is mainly biogenic and not detrital (Ross and Bustin, in review), and the diagenesis of biogenic silica plays an important role in preserving or destroying the pore space by secondary cementation (silica-dissolution and re-precipitation; Volpi et al., 2003). Such processes do not preclude gas sorption in quartz-rich shales as there are micropore surfaces within the organic matter upon which gas can sorb (Sections 3.2 and 3.6). The total porosity is a function of meso- and macropores, not micropores, as evident by the good correlation between porosity (measured by Hg porosimetry) and N_2 BET surface area. Micropores measured using low pressure CO_2 analyses are not quantified due to the inability of Hg to penetrate restricted pore throats (Webb and Orr, 1997).

Despite the irrelevance of the meso- and macropore structure and total porosity to gas sorption (controlled by microporosity), an understanding of these attributes is important to predicting total gas capacities. A significant proportion of the total gas content in shale gas reservoirs is free-gas (non-sorbed gas occupying open pores), especially at high reservoir temperatures (e.g. 100 °C; Ross and Bustin, 2008). During production, free-gas co-mingles with sorbed gas, explaining the over-saturation of shale gas reservoirs (Bustin, 2005a,b; Montgomery et al., 2005).

5. Conclusions

A variety of pore structure analyses have been applied to a suite of organic-poor and organic-rich shales of different thermal maturation and inorganic composition, to determine the fundamental controls on gas capacities in fine-grained marine strata. The following conclusions have been reached:

(1) The organic fraction in shales is an important control on CH_4 storage capacity, shown by positive correlations between TOC and sorbed gas.
(2) For thermally immature Jurassic shales enriched with matrix bituminite, no relationship exists between TOC and D–R CO_2 micropore volumes or N_2 BET surface areas, indicating surface area alone is not the sole determiner of CH_4 capacity. A component of solute CH_4 within the internal structure of the matrix bituminite is an important gas storage mechanism in Jurassic shales.
(3) Thermally mature shales have larger D–R CO_2 micropore volumes and N_2 BET surface areas per wt% TOC. Hence the ratio of sorbed gas to TOC is greater in thermally mature strata (D–M) than immature strata.
(4) The relationship (or ratio) between organics and CH_4 sorption is affected by mineral matter. Clay minerals such as illite have micropore structures capable of sorbing gas. Mercury porosimetry analyses show that clay-rich shales have a significant percentage of mesoporosity (unimodal pore size distribution in the mesopore range).
(5) Total porosity increases with decreasing Si/Al ratios, a reflection of the porosity associated with clay mineral phases. Conversely high Si/Al (quartz-rich) shales have lower total porosities and tight-rock characteristics.

The results of this research highlight the pore structure complexity of shales and mudrocks. Due to multi-modal pore size distributions and surface area heterogeneities in the nanometre scale, there is difficulty predicting sorbed gas capacities of shales based on TOC contents and maturation levels alone. Shales contain a variety of organic and inorganic materials with multifarious pore networks, which vary from one shale formation to another and within a formation itself. Hence the ability to establish a model of shale gas reservoir capacity is challenging and the prediction of CH_4 capacities is problematic.

Future research on gas sorption in shales will require a multifaceted approach, addressing the effects of other reservoir parameters including moisture and temperature. Moisture is known to influence gas sorption in coals and shales (acting as a dilutent), but its relationship to the pore structure in shales is unclear.

References

Altin, O., Özbelge, Ö., Dogu, T., 1999. Effect of pH in an aqueous medium on the surface area, pore size and distribution, density and porosity of montmorillonite. J. Colloid Interface Sci. 217, 19–27.

Aringhieri, R., 2004. Nanoporosity characteristics of some natural clay minerals and soils. Clays Clay Miner. 52, 700–704.

ASTM, 2004. Test for Equilibrium Moisture of Coal at 96 to 97% Relative Humidity and 30 °C, D1412-04.

Aylmore, L.A.G., 1974. Gas sorption in clay mineral systems. Clays Clay Miner. 22, 175–183.

Aylmore, L.A.G., Quirk, J.P., 1967. The micropore size and distribution of clay mineral systems. J. Soil Sci. 18, 1–17.

Azmi, A.S., Yusup, S., Muhamad, S., 2006. The influence of temperature on adsorption capacity of Malaysian coal. Chem. Eng. Process. 45, 392–396.

Brunauer, S., Emmet, P.H., Teller, E., 1938. Adsorption of gases in multimolecular layers. J. Am. Chem. Soc. 60, 309.

Brunauer, S., Deming, L.S., Deming, W.S., Teller, E., 1940. On a theory of van der Waals adsorption of gases. J. Am. Chem. Soc. 62, 1723–1732.

Burggraaf, A.J., 1999. Single gas permeation of thin zeolite (MFI) membranes: theory and analysis of experimental observations. J. Membr. Sci. 155, 45–65.

Bustin, R.M, 2005a. Gas shale tapped for big play. In: AAPG Explorer, February 5–7.

Bustin, R.M., 2005b. Factors influencing the reservoir capacity of gas shales and coals (abs.): key note address. In: Gussow Conference, Canadian Society of Petroleum Geologists, March 10, 2005, Banff, Alberta, p. 5.

Bustin, R.M., Clarkson, C.R., 1998. Geological controls on coalbed methane reservoir capacity and gas content. Int. J. Coal Geol. 38, 3–26.

Chalmers, G.R.L., Bustin, R.M., 2007a. The organic matter distribution and methane capacity of the Lower Cretaceous strata of northeastern British Columbia. Int. J. Coal Geol. 70, 223–239.

Chalmers, G.R.L., Bustin, R.M., 2007b. On the effects of petrographic composition on coalbed methane sorption. Int. J. Coal Geol. 69, 288–304.

Cheng, A.L., Huang, W.L., 2004. Selective adsorption of hydrocarbon gases on clays and organic matter. Org. Geochem. 35, 413–423.

Clarkson, C.R., Bustin, R.M., 1996. Variation of micropore capacity and size distribution with composition in bituminous coal of the Western Canadian Sedimentary Basin. Fuel 75, 1483–1498.

Clarkson, C.R., Bustin, R.M., 1999. The effect of pore structure and gas pressure upon the transport properties of coal: a laboratory and modeling study. 1. Isotherms and pore volume distributions. Fuel 78, 1333–1344.

Crosdale, P.J., Beamish, B.B., Valix, M., 1998. Coalbed methane sorption related to coal composition. Int. J. Coal Geol. 35, 147–158.

Dewhurst, D.N., Aplin, A.C., Sarda, J.P., 1999a. Influence of clay fraction on pore-scale properties and hydraulic conductivity of experimentally compacted mudstones. J. Geophys. Res. 104, 29261–29274.

Dewhurst, D.N., Yang, Y., Aplin, A.C., 1999b. Permeability and fluid flow in natural mudstones. In: Aplin, A.C., Fleet, A.J., Macquaker, J.H.S. (Eds.), Muds and Mudstones: Physical and Fluid Flow Properties. Geological Society, London, Special Publications, pp. 125–136.

Dubinin, M.M., 1975. Physical adsorption of gases and vapours in micropores. In: Cadenhead, D.A., Danielli, J.F., Rosenberg, M.D. (Eds.), Progress in Surface and Membrane Science, vol. 9. Academic Press, New York, pp. 1–70.

Dubinin, M.M., 1989. Fundamentals of the theory of adsorption in micropores of carbon adsorbents: characteristics of their adsorption properties and microporous structures. Pure Appl. Chem. 61, 1841–1843.

Dubinin, M.M., Stoeckli, H.E., 1980. Homogeneous and heterogeneous micropore structures in carbonaceous adsorbents. J. Coll. Surface Sci. 75, 34–42.

Duffy, J.R., Smith, N.O., Nagy, B., 1961. Solubility of natural gases in aqueous salt solutions – I: liquidus surfaces in the system CH_4–H_2O–$NaCl_2$–$CaCl_2$ at room temperatures and at pressures below 1000 psia. Geochim. Cosmochim. Acta 24, 23–31.

Eseme, E., Littke, R., Krooss, B.M., 2006. Factors controlling the thermo-mechanical deformation of oil shales: implications for compaction of mudstones and exploitation. Mar. Pet. Geol. 23, 715–734.

Fripiat, J.J., Cruz, M.I., Bohor, F., Thomas Jr., J., 1974. Interlamellar adsorption of carbon dioxide by smectites. Clays Clay Miner. 22, 23–30.

Gan, H., Nandie, S.P., Walker Jr., P.L., 1972. Nature of porosity in American coals. Fuel 51, 272–277.

Gil, A., Massinon, A., Grange, P., 1995. Analysis and comparison of the microporosity in Al-, Zr- and Ti-pillared clays. Microporous Mater. 4, 369–378.

Gregg, S.J., Sing, K.S.W., 1982. Adsorption Surface Area and Porosity. Academic Press, New York.

Hildenbrand, A., Krooss, B.M., Busch, A., Gaschnitz, R., 2006. Evolution of methane sorption capacity of coal seams as a function of burial history – a case study from the Campine Basin, NE Belgium. Int. J. Coal Geol. 66, 179–203.

Joubert, J.I., Grein, C.T., Bienstock, D., 1973. Sorption of methane in moist coal. Fuel 52, 181–185.

Joubert, J.I., Grein, C.T., Bienstock, D., 1974. Effect of moisture on the methane capacity of American coals. Fuel 53, 186–191.

Katsube, T.J., Williamson, M.A., 1994. Effects of diagenesis on shale nanopore structure and implications for sealing capacity. Clay Miner. 29, 451–461.

Katsube, T.J., Cox, W.C., Issler, D.R., 1998. Porosity characteristics of shale formations from the Western Canadian Sedimentary Basin. In: Current Research 1998-E, Geological Survey of Canada, pp. 63–74.

Krooss, B.M., van Bergen, F., Gensterblum, Y., Siemons, N., Pagnier, H.J.M., David, P., 2002. High-pressure methane and carbon dioxide adsorption on dry and moisture-equilibrated Pennsylvanian coals. Int. J. Coal Geol. 51, 69–92.

Lamberson, M.N., Bustin, R.M., 1993. Coalbed methane characteristics of Gates formation coals, northeastern British Columbia: effect of maceral composition. AAPG Bull. 77, 2062–2076.

Langmuir, I., 1918. The adsorption of gases on plane surfaces of glass, mica and platinum. J. Am. Chem. Soc. 40, 1403–1461.

Larsen, J.W., Hall, P., Wernett, P.C., 1995. Pore structure of the Argonne Premium Coals. Energy Fuels 9, 324–330.

Law, B.E., Curtis, J.B., 2002. Introduction to petroleum systems. AAPG Bull. 86, 1851–1852.

Laxminarayana, C., Crosdale, P.J., 1999. Role of coal type and rank on methane sorption characteristics of Bowen Basin, Australia Coals. Int. J. Coal Geol. 40, 309–325.
Laxminarayana, C., Crosdale, P.J., 2002. Controls on methane sorption capacity of Indian Coals. AAPG Bull. 86, 201–212.
Levy, J.H., Day, S.J., Killingley, J.S., 1997. Methane capacities of Bowen Basin coals related to coal properties. Fuel 76, 813–819.
Lloyd, M.K., Conley, R.F., 1970. Adsorption studies on kaolinites. Clays Clay Miner. 18, 37–46.
Lu, X.C., Li, F.-C., Watson, A.T., 1995. Adsorption measurements in Devonian shales. Fuel 74, 599–603.
Majorowicz, J.A., Jessop, A.M., Lane, L.S., 2005. Regional heat flow pattern and lithospheric geotherms in northeastern British Columbia and adjacent Northwest Territories, Canada. Bull. Can. Petr. Geol. 53, 51–66.
Manger, K.C., Oliver, S.J.P., Curtis, J.B., Scheper, R.J., 1991. Geologic influences on the location and production of Antrim shale gas, Michigan Basin. SPE 21854, 511–519.
Marsh, H., 1989. Adsorption methods to study microporosity in coals and carbons – a critique. Carbon 25, 49–58.
Mastalerz, M., Gluskoter, H., Rupp, J., 2004. Carbon dioxide and methane sorption in high volatile bituminous coals from Indiana, USA. Int. J. Coal Geol. 60, 43–55.
Mondol, N.H., Bjørlykke, K., Jahren, J., Høeg, K., 2007. Experimental mechanical compaction of clay mineral aggregates – changes in physical properties of mudstones during burial. Mar. Pet. Geol. 24, 289–311.
Montgomery, S.L., Jarvie, D.M., Bowker, K.A., Pallastro, R.M., 2005. Mississippian Barnett Shale, Fort Worth basin, north-central Texas: Gas-shale play with multi-trillion cubic foot potential. AAPG Bull. 89, 155–175.
Morrow, D.W., Potter, J., Richards, B., Goodarzi, F., 1993. Paleozoic burial and organic maturation in the Liard Basin Region, northern Canada. Bull. Can. Pet. Geol. 41, 17–31.
Pollastro, R.M., 2007. Total petroleum system assessment of undiscovered resources in the giant Barnett Shale continuous (unconventional) gas accumulation, Fort Worth Basin, Texas. AAPG Bull. 91, 551–578.
Potter, J., Goodarzi, F., Morrow, D.W., Richards, B.C., Snowdon, L.R., 2000. Organic Petrology, Thermal Maturity, and Rock-Eval/TOC Data for Upper Paleozoic Strata from Selected Wells between 60° and 61°N and 122°W and 123°30′ SW, District of Mackenzie. Geological Survey of Canada Open File Report 3925.
Potter, J., Goodarzi, F., Morrow, D.W., Richards, B.C., Snowdon, L.R., 2003. Organic Petrology, Thermal Maturity and Rock-Eval/TOC Data for Upper Paleozoic to Upper Cretaceous Strata from Wells near Liard River, Northeast British Columbia. Geological Survey of Canada Open File Report 1751.
Prinz, D., Littke, R., 2005. Development of the micro- and ultramicroporous structure of coals with rank as deduced from the accessibility of water. Fuel 84, 1645–1652.
Reucroft, P.J., Patel, K.B., 1983. Surface area and swellability of coal. Fuel 62, 279–284.
Rouquerol, J., Avnir, D., Fairbridge, C.W., Everett, D.H., Haynes, J.H., Pernicone, N., Ramsay, J.D.F., Sing, K.S.W., Unger, K., 1994. Recommendations for the characterization of porous solids, International Union of Pure and Applied Chemistry. Pure Appl. Chem. 68, 1739–1758.
Ross, D.J.K., 2004. Sedimentology, geochemistry and gas shale potential of the Early Jurassic Gordondale Member, northeastern British Columbia. MSc thesis, unpublished, 147 pp.
Ross, D.J.K., Bustin, R.M., 2006. Sediment geochemistry of the Lower Jurassic Gordondale Member, northeastern British Columbia. Bull. Can. Pet. Geol. 54, 337–365.
Ross, D.J.K., Bustin, R.M., 2007. Shale gas potential of the Lower Jurassic Gordondale Member, northeastern British Columbia, Canada. Bull. Can. Pet. Geol. 55, 51–75.
Ross, D.J.K., Bustin, R.M. Investigating the use of sedimentary geochemical proxies for paleoenvironments of thermally mature organic-rich strata: examples from Devonian-Mississippian strata, Western Canadian Sedimentary Basin. Chem. Geol., in review.
Ross, D.J.K., Bustin, R.M., 2008. Characterizing the shale gas resource potential of Devonian-Mississippian strata in the Western Canada sedimentary basin: application of an integrated formation evaluation. AAPG Bull. 92, 87–125.
Schlömer, S., Krooss, B.M., 1997. Experimental characterisation of the hydrocarbon sealing efficiency of cap rocks. Mar. Pet. Geol. 14, 565–580.
Sing, K.S.W., Everett, D.H., Haul, R.A.W., Moscou, L., Pierotti, R.A., Rouquerol, J., Siemieniewska, T., 1985. Reporting physiosorption data for gas/solid systems with special reference to the determination of surface area and porosity. Pure Appl. Chem. 57, 603–619.
Stach, E., Mackowsky, M.T., Teichmüller, M., Taylor, G.A., Chandra, D., Leichmüller, R., 1982. Coal Petrology, second ed., Berlin. Stuttgart (Gebrüder Borntträger).
Stasiuk, L.D., Fowler, M.G., 2002. Thermal Maturity Evaluation (Vitrinite and Vitrinite reflectance Equivalent) of Middle Devonian, Upper Devonian and Devonian–Mississippian Strata in the Western Canada Sedimentary Basin. Geological Survey of Canada, Open File Report 4341.
Stasiuk, L.D., Fowler, M.G., 2004. Organic facies in Devonian and Mississippian strata of Western Canada sedimentary basin; relation to kerogen type, paleoenvironment, and paleogeography. Bull. Can. Pet. Geol. 52, 234–255.
Svrcek, W.Y., Mehrotra, A.K., 1982. Gas solubility, viscosity and density measurements for Athabasca bitumen. J. Can. Pet. Technol. 21, 31–38.
Teichmüller, M., 1986. Organic petrology of source rocks, history and state of the art. Org. Geochem. 10, 581–599.
Teichmüller, M., Ottenjann, K., 1977. Art und diagenese von liptiniten und lipoiden stiffen in einem erdölmuttergestein auf grund fluoreszenzmikroskopischer untersuchungen. Erdöl Kohle 30, 387–398.
Unsworth, J.F., Fowler, C.S., Jones, L.F., 1989. Moisture in coal: 2. Maceral effects on pore structure. Fuel 68, 18–26.
Volpi, V., Camerlenghi, A., Hillenbrand, C.-D., Rebesco, M., Ivaldi, R., 2003. Effects of biogenic silica on sediment compaction and slope stability on the Pacific margin of the Antarctic Peninsula. Basin Res. 15, 339–363.
Wang, C.C., Juang, L.C., Lee, C.K., Hsu, T.C., Lee, J.F., Chao, H.P., 2004. Effects of exchanged surfactant cations on the pore structure and adsorption characteristics of montmorillonite. J. Colloid Interface Sci. 280, 27–35.
Washburn, E.W., 1921. Note on the method of determining the distribution of pore sizes in a porous material. Proc. Natl. Acad. Sci. U.S.A. 7, 115–116.
Webb, P.A., Orr, C., 1997. Analytical Methods in Fine Particle Technology. Micromeritics Instrument Corporation Publishers, Norcross, pp. 161–162.
Wright, G.N., McMechan, M.E., Potter, D.E.G., 1994. Structure and architecture of the Western Canada Sedimentary Basin – Chapter 3. In: Mossop, G.D., Shetsen, I. (Comps.). Geological Atlas of the Western Canada Sedimentary Basin. Canadian Society of Petroleum Geologists and Alberta Research Council, pp. 25–40.
Yalçin, E., Durucan, S., 1991. Methane capacities of Zonguldak coals and the factors affecting methane adsorption. Min. Sci. Technol. 13, 215–222.
Yang, Y., Aplin, A.C., 1998. Influence of lithology and compaction on the pore size distribution and modelled permeability of some mudstones from the Norwegian margin. Mar. Pet. Geol. 15, 163–175.
Yee, D., Seidle, J.P., Hanson, W.B., 1993. Gas sorption on coal measurements and gas content. In: Law, B.E., Rice, D.D. (Eds.), Hydrocarbons from Coal, AAPG Studies in Geology, pp. 203–218 (Chapter 9).